JGR Atmospheres

RESEARCH ARTICLE
10.1029/2021JD034903

Key Points:

- Models simulate an equatorward shift of the Asian and disappearance of the North American monsoon anticyclones in 4 × CO_2 simulations
- Changes in the upper troposphere and lower stratosphere anticyclones are dominated by the effect of indirect SST warming by CO_2
- Circulation changes due to 4 × CO_2 result in a significant reduction of ozone in the northern tropics at 100 hPa

Supporting Information:

Supporting Information may be found in the online version of this article.

Correspondence to:

O. V. Tweedy,
olgatweedy@gmail.com

Citation:

Tweedy, O. V., Oman, L. D., Waugh, D. W., Schoeberl, M. R., Douglass, A. R., & Li, F. (2021). Response of the upper-level monsoon anticyclones and ozone to abrupt CO_2 changes. *Journal of Geophysical Research: Atmospheres*, *126*, e2021JD034903. https://doi.org/10.1029/2021JD034903

Received 11 MAR 2021
Accepted 1 OCT 2021

Response of the Upper-Level Monsoon Anticyclones and Ozone to Abrupt CO_2 Changes

Olga V. Tweedy[1,2], Luke D. Oman[2], Darryn W. Waugh[3], Mark R. Schoeberl[4], Anne R. Douglass[2], and Feng Li[1,2]

[1]Universities Space Research Association, Columbia, MD, USA, [2]NASA Goddard Flight Center, Greenbelt, MD, USA, [3]Department of Earth and Planetary Sciences, JHU, Baltimore, MD, USA, [4]Science and Technology Corporation, Columbia, MD, USA

Abstract The summer monsoon anticyclones are the dominant climatological features of the Northern Hemispheric (NH) summertime circulation in the upper troposphere and lower stratosphere (UTLS). However, the response of these anticyclones to the increased levels of CO_2 remains highly uncertain, as does the impact on the distribution of UTLS ozone and other tracers. This study examines the response of the NH summertime monsoon anticyclones and UTLS ozone to the abrupt increase in CO_2 forcing using output from a suite of coupled ocean–atmosphere general circulation model simulations. These models show an equatorward shift of the Asian summer monsoon anticyclone, a weakening of the North American summer monsoon anticyclone, and a stronger westerly flow penetrating deep into the tropics above the Pacific Ocean and North America. We use additional idealized experiments from atmosphere-only general circulation models with prescribed SSTs and sea ice concentration to isolate the direct atmospheric radiative effects from the indirect effect of SST warming on the UTLS monsoon anticyclones. Comparison between atmosphere-only and coupled ocean–atmosphere experiments shows that SST warming is the principal mechanism producing UTLS monsoonal circulation changes. The 4 × CO_2 experiments result in a significant reduction up to 40%–50% of the UTLS ozone in the northern tropics, which could have an impact on radiative balance near the surface.

1. Introduction

The Asian and North American summer monsoons are the dominant climatological features of the Northern Hemispheric (NH) summertime circulation. The monsoons shape precipitation and regional circulation patterns worldwide, providing more than one-half of the global population with moisture (Wang & Ding, 2008; Wang et al., 2013). These monsoon circulations consist of cyclonic flow and convergence in the lower troposphere and intense anticyclonic circulations and divergence in the upper troposphere - lower stratosphere (UTLS). The cyclonic and anticyclonic circulations are coupled by persistent deep convection over South Asia (Tibetan Plateau) and North America (Colorado Plateau) during NH summer. Both UTLS anticyclones arise as response to diabatic heating within their respective hemispheres (Gill, 1980; Hoskins & Rodwell, 1995; Siu & Bowman, 2019) and are bounded by the subtropical westerly jet in the north and easterly jet in the south.

The Asian summer monsoon (ASM) and North American summer monsoon (NASM) anticyclones have substantial intraseasonal variability in strength and location. The ASM anticyclone is centered around 30°N and 70°E and is evident in the UTLS by May. It shifts northward, peaks in strength, and extends over the large areas of eastern hemisphere by July, weakens in September, and disappears in October (Basha et al., 2020; Garny & Randel, 2013).

The NASM anticyclone is not as strong or persistent as its Asian counterpart (Chen, 2003; Dunkerton, 1995). A nascent NASM forms in late May off the Pacific coast of Central America, near the eastern Pacific intertropical convergence zone, then it moves northward along the Pacific coast of Mexico until it is centered near northwestern Mexico extending into the southwestern United States (Douglas et al., 1993; Schoeberl et al., 2020). The NASM anticyclone becomes mature in July and August and gradually decays from late September (Vera et al., 2006).

The edges of the UTLS monsoon anticyclones serve as horizontal transport barriers for constituents, resulting in elevated aerosol, water vapor (H_2O) and carbon monoxide (CO) concentration, and low ozone (Park et al., 2007; Randel et al., 2015). These constituents are trapped inside anticyclones. Outside of these systems, the circulation along the edges of the anticyclones brings chemical constituents from the extratropics into the tropics and vice versa, producing hemispheric and zonal asymmetries in trace gases (Stolarski et al., 2014; Tweedy et al., 2017). Furthermore, strong cross-equatorial winds at the southward edge of the monsoon anticyclone transport NH surface air and trace species into the SH via meridional advection and/or through eddy-driven processes like shedding of PV (G. Chen et al., 2017; Orbe et al., 2016; Popovic & Plumb, 2001). Thus, variability in the strength and location of the monsoon anticyclones affects the regional distribution of chemical constituents such as ozone, impacting regional surface climate (Xia et al., 2018, and references therein).

As the carbon dioxide (CO_2) concentration is projected to increase in the 21st century, the monsoon systems are expected to respond, but that response remains highly uncertain. Previous research related to the regional response of the monsoons to climate warming often focused on the tropospheric circulation and precipitation. Pascale et al. (2019) concluded that uncertainty in the response mechanisms to global warming remains high, especially for the NASM. They attributed the ambiguous response of the NASM to systematic global model biases (e.g., sea-surface temperature biases) and inadequate horizontal resolution, thus limiting confidence in future projections. Most studies of the UTLS circulation response to increased greenhouse gases (GHGs) focus on the zonally and/or annually averaged characteristics (Abalos et al., 2017; Garcia & Randel, 2008; Orbe et al., 2020), which leaves a response of the summer monsoon anticyclones unexplored. Changes in monsoons would be expected to significantly influence regional climate, as well as the UTLS circulation and composition.

An increase in the GHGs impacts the climate system in two ways, through direct radiative forcing and indirect SST warming. The direct radiative effect of increased CO_2 levels results in enhanced downward infrared radiation, which warms land and oceans. However, the oceans warm more slowly than the land due to the higher heat capacity of water, leading to an increased land-ocean temperature contrast. Thus, direct CO_2 forcing modulates land temperatures and the other climate variables (Kamae et al., 2015; Sherwood et al., 2015), while changes in the SSTs influence the global climate via dynamic and thermodynamic processes (Bony et al., 2013; Ma et al., 2012; Shaw & Voigt, 2015).

Previous studies showed that direct atmospheric radiative forcing due to the CO_2 increase and indirect SST warming can impose competing effects on tropospheric monsoon circulation, e.g., a tug-of-war (Li & Ting, 2017; Qu & Huang, 2020; Shaw & Voigt, 2015). In response to direct CO_2 radiative forcing, subcloud equivalent potential temperature contrasts between land and ocean increase, resulting in a stronger moisture convergence and more intense lower-level Asian monsoon cyclone. In contrast, the response to SST warming involves decrease in the land-ocean temperature contrast, leading to a low–level moisture divergence around Asia and a weaker Asian monsoon circulation. These competing effects explain why the response of the Asian monsoon cyclone in the lower troposphere to increased CO_2 is weak (Shaw & Voigt, 2015). Qu and Huang (2020) used outputs from climate models to show that the uniform sea surface warming reduces the ascending motion of the air over the Tibetan Plateau, which is partially offset by the CO_2 direct impact. The combined effect of the two causes only a small net change in ascending motion. While circulation compensation in the troposphere that occur in response to opposite land-sea temperature contrasts is a robust result among climate models in the Asian region such compensation does not appear to be robust in the NASM response to global warming (Shaw & Voigt, 2015) and the contributions (or even signs) of two effects on the UTLS upper-level monsoon anticyclones are unknown.

In this study, the response of the NH summer monsoon anticyclones and ozone to quadrupled CO_2 is examined using monthly output from a suite of coupled ocean–atmosphere general circulation models. We focus on the zonally resolved circulation changes in the UTLS, which to our knowledge haven't been rigorously examined by previous studies. Furthermore, we investigate relative contributions of the direct CO_2 radiative forcing and indirect sea surface temperature warming to the circulation changes using a suite of simulations from atmospheric general circulation models with prescribed sea surface temperatures.

We aim to answer the following questions:

Table 1
Overview of Models Participating in This Study

Model	Strat. chemistry	Horizontal grid (lon x lat), vert. levels, top level	References
1. Community Earth System Model version 2 (CESM2)	Prescribed	0.9° x 1.25°, 32 levels, top level 2.25 hPa	Danabasoglu et al. (2019)
2. Community Earth System Model version 2 (CESM2) – WACCM	Interactive	0.9° x 1.25°, 70 levels, top level 4.5e−06 hPa	Danabasoglu (2019b); Danabasoglu (2019a)
3. National Centre for Meteorological Research (CNRM-CM6)	Simplified online scheme	1.4° x 1.4°, 91 levels, top level 78.4 km	Voldoire (2018b); Voldoire (2018a)
4. National Centre for Meteorological Research (CNRM-ESM2)	Interactive	1.4° x 1.4°, 91 levels, top level 78.4 km	Seferian (2018b); Seferian (2018a)
5. The Energy Exascale Earth System Model (E3SM-1-0)	Simplified online scheme	1°xl°, 72 levels, top level 0.1 hPa	Bader et al. (2019a, 2019b)
6. The Geophysical Fluid Dynamics Laboratory – Earth System Model 4 (GFDL-ESM4)	Interactive	1°xl°, 49 levels, top level 1 Pa	Krasting et al. (2018a, 2018b)
7. Goddard Institute for Space Studies E2-1-G (GISS-E2-1-G)	Interactive	2.5°x2°, 40 levels, top level 0.1 hPa	NASA/ GISS (2018a, 2018b)
8. Meteorological Research Institute Earth System Model version 2.0 (MRI-ESM2-0)	Interactive	1.125° x x1.12°, 80 levels, top level 0.01 hPa	Yukimoto et al. (2019a, 2019b)
9. UK Eath System Model version 1 (UKESM1-0-LL)	Interactive	1.875°x1.25°, 85 levels, top level 85 km	Tang et al. (2019a, 2019b)
10. Hadley Centre Global Environment Model version 3 (HadGEM3-GC31-LL)	Prescribed	1.875°x1.25°, 85 levels, top level 85 km	Ridley et al. (2019a, 2019b)
11. Goddard Earth Observing System Chemistry Climate Model (GEOSCCM)	Interactive	1°xl°, 72 levels, top level 0.01hPa	Li and Newman (2020)

1. How do the ASM and NASM anticyclones respond to the abrupt changes in CO_2 in the coupled ocean–atmosphere global model?
2. How does the upper-level monsoonal circulation respond to the SST increase and direct radiative forcing that accompanies quadrupled CO_2?
3. What is the impact of the circulation changes on UTLS ozone?

In the next section, we briefly describe models, simulations, and methodology. The NH summer response of the UTLS circulation to the quadrupled CO_2 in the coupled ocean–atmosphere General Circulation Models (GCMs) is examined in Section 3. In Section 4, we evaluate the contributions of the direct radiative effect of CO_2 and indirect SST warming to the total changes in the UTLS circulation and NASM and ASM anticyclones in particular. UTLS ozone response to the increase in GHGs is explored in Section 5. Discussion of results and conclusions are in Section 6.

2. Models and Methods

2.1. Coupled Model Simulations

The response of the NH summertime UTLS circulation to the abrupt increase in CO_2 forcing is examined using monthly output from 11 coupled ocean–atmosphere GCMs, 10 of which participated in the newest phase of the Coupled Model Intercomparison Project (CMIP)-Phase 6, CMIP6 (Eyring et al., 2016). These models, their horizontal resolution, and corresponding references are listed in Table 1. We analyzed two different forcing experiments from each of the coupled models: a control and an abrupt carbon dioxide quadrupling ($4 \times CO_2$). Each $4 \times CO_2$ scenario consists of 150 model years where CO_2 concentration was abruptly increased four times from the level of the control simulation and then held constant throughout the entire length of the simulation. Most control experiments are integrated more than 100 years under fixed preindustrial conditions. For GEOSCCM (Model 11) we used a 50-year baseline simulation under fixed year-2000 conditions. Since all other forcings in the $4 \times CO_2$ simulations are identical to those in control simulation,

it is possible to isolate robust changes in the summertime UTLS circulation and their impacts on ozone. Thus, the abrupt $4 \times CO_2$ forcing simulations allow for a mechanistic look into the response characteristics of GCMs that can be unambiguously attributed to an increase in CO_2 concentrations. Since the circulation and ozone responses to $4 \times CO_2$ after 100 years are at/or near equilibrium (not shown), we defined these responses as differences between the climatology obtained from the last 50 years of the $4 \times CO_2$ run and the climatological averages of the last 100 years in the control run.

Our choice of coupled models from CMIP6 is primarily based on the availability of interactive/predictive ozone fields (see Table 1). We use the nine out of 11 models listed in Table 1 that have predictive ozone. Ozone fields are prescribed in remaining two models, CESM2 and HadGEM3-GC31-LL; therefore, they are not used for ozone analyses. Seven of nine models with predictive ozone have fully coupled, online interactive stratospheric chemistry (CESM2-WACCM, GEOSCCM, CNRM-ESM2-1, GFDL-ESM4, MRI-ESM2-0, GISS-E2-1-G, and UKESM1-0-LL) while two others (CNRM-CM6-1 and E3SM-1-0) use a simplified chemistry scheme.

2.2. Atmosphere-Only Model Simulations

The net response of the coupled ocean–atmosphere system includes fast and slow components related to the direct atmospheric radiative effect of CO_2 and indirect SST warming. To separate fast and slow components, we used simulations from three atmosphere-only GCMs with prescribed SSTs and sea ice concentration. The following experiments are available and archived in the CMIP6 for CESM2, CNRM-CM6, and HadGem3:

1. piSSTice (i.e., "preindustrial CO_2 and SSTs"): An atmosphere-only model experiment with monthly- and interannually- varying SSTs, sea-ice, atmospheric constituents, and any other necessary boundary conditions taken from each model's preindustrial control run.
2. piSSTice+$4 \times CO_2$, (i.e., "direct radiative forcing of quadrupled CO_2"): Same as piSSTice, but CO_2 is quadrupled.
3. a4SSTice (i.e., "SST warming forcing"): Same as piSSTice, but with SSTs and sea-ice taken from years 111–140 of each model's abrupt-$4 \times CO_2$ experiment instead of from Control.
4. a4SSTice+$4 \times CO_2$, (i.e., "both forcings"): Same as a4SSTice, but CO_2 is quadrupled.

Amongst the three models participating in these atmosphere-only experiments, only CNRM-CM6 has predictive chemistry with ozone.

2.3. Methods

The summer monsoon anticyclones are examined using horizontal stream function at 100 hPa. The horizontal stream function is obtained using the python library windspharm, which performs computations on global wind fields in spherical geometry (Dawson, 2016). After computing stream function using three-dimensional fields of zonal (U) and meridional (V) winds for each model separately, we interpolated stream function and horizontal winds to a common 1° longitude by 1° latitude grid to produce the multi-model averages. The stream function is used as in the previous studies to evaluate the strength and location of the ASM anticyclone (Tweedy et al., 2018; Yan et al., 2018). To examine the strength, we averaged a stream function over the regions of the ASM (20°N – 40°N and 40°E – 100°E) and NASM (25°N–40°N and 90°W–120°W) anticyclones. The latitude where the stream function is maximal inside the ASM anticyclone (i.e., center of the ASM anticyclone) is used to estimate changes in the location due to increased CO_2. Although the ASM and NASM anticyclones persist from May to September, our analysis focuses on July-August averages when both anticyclones are in their mature stages. This allows us to detect a robust signal and avoid cancellations associated with strong sub-seasonal variations in strength and location of the UTLS anticyclones. The seasonal strength of the ASM and NASM anticyclones is estimated as a difference between area average stream function (as defined above) during July-August and April-May at 100 hPa. A statistical significance of the differences between two types of experiments (e.g., "Control" and "$4 \times CO_2$") from each model is accessed via Student's t test at the 95% confidence level.

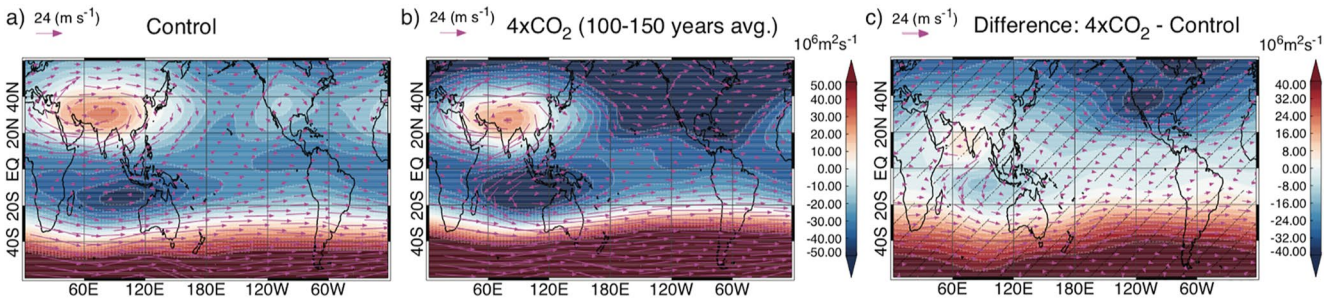

Figure 1. Stream function (shaded) and wind vectors at 100 hPa during July-August averaged over 11 coupled ocean–atmosphere models. (a) Climatological average of the Control simulations; (b) 50-year average of perturbed $4 \times CO_2$ simulations 100 years after quadrupled CO_2 forcing was applied to the Control; (c) the difference between $4 \times CO_2$ and control simulations. Hatching indicates regions where at least 9 out of 11 models agree on the sign of change. Reference wind vector is 24 ms^{-1}.

3. Response of 100 hPa Global Circulation to Quadrupled CO_2

We started by examining the response of the 100 hPa circulation to quadrupled CO_2 concentrations in the coupled models. Figure 1 shows a multi-model mean of horizontal stream function (shaded) and horizontal winds (arrows) averaged over July and August for Control, $4 \times CO_2$ simulations, and their difference, "$4 \times CO_2$ – Control". In the Control simulation, the ASM and NASM anticyclones can be seen by enclosed/circular contours above Asia and North America; the NASM anticyclone is much weaker than its Asian counterpart (Figure 1a). While the initial strength of the ASM and NASM anticyclones varies widely among individual models (see Figure S1a in Supporting Information S1), there is a remarkably good agreement on several aspects of the UTLS response to the abrupt increase in CO_2.

First, positive stream function differences at the northern tropical Indian Ocean between Control and $4 \times CO_2$ simulations (Figure 1c) indicate the equatorward shift in the ASM anticyclone. As shown in Figure 2a, each coupled model's control simulation (in red) shows a consistently more northward center of the ASM anticyclone than during last 50 years of the $4 \times CO_2$ simulations (in black). The location of the ASM anticyclone's center in the Control experiments vary among the models from ~28°N in GEOSCCM to ~32°N in CNRM-CM6 (for comparison, the modern–day climatological value from MERRA2 reanalyses is ~31°N, shown as dashed horizontal line). While there is a spread among models in the initial location of the

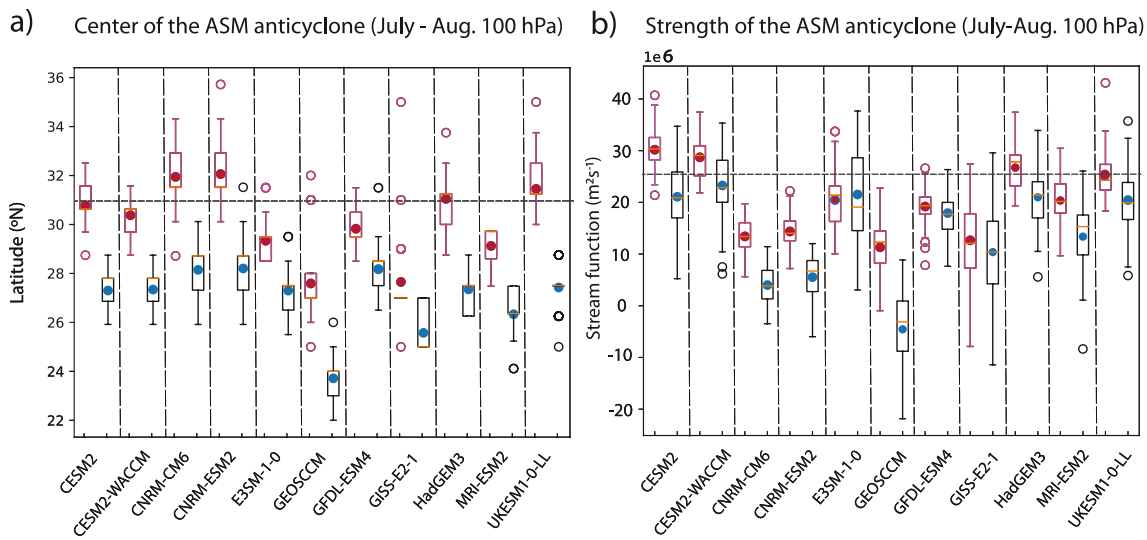

Figure 2. (a) A latitude of maximum in 100 hPa stream function above Asia and (b) 100 hPa stream function, averaged over the area of ASM anticyclone (20°N–40°N and 40°E–100°E) in July–August from 11 coupled ocean–atmosphere models with the Control and $4 \times CO_2$ simulations shown in red and black respectively. Shown are median (horizontal line), mean (filled red and blue dots), 25th–75th percentiles (box), minimum and maximum values (whiskers), and outliers (dots).

anticyclone's center, and magnitude of the shift (from as little as 1.6° in the GFDL-ESM4 to as much as 4° in UKESM1), they all show a robust and statistically significant change in the same direction (positive stream function differences at the northern tropical Indian Ocean are free of hatching in Figure S1c of Supporting Information S1 for every model).

Contrarily to the shift in the ASM anticyclone, which is a robust and significant response among 11 coupled models, the changes in the strength of circulation above Asia due to quadrupled CO_2 are model dependent. Area-averaged stream function from individual coupled models either remains the same or weakens due to $4 \times CO_2$ (Figure 2b) with a weak multi-model response (compare Figures 1a and 1b). In the lower troposphere, Shaw and Voigt (2015) also showed a weak response of the Asian monsoon circulation to the increased GHGs in climate models, which often don't agree on the sign of the change. While the response of the circulation above Asia in the UTLS is also weak, there is a better agreement among the coupled models on the sign of the change (e.g., weakening of the ASM anticyclone in seven out of 11 models and no significant change in the strength in four models).

Furthermore, Figure 1b shows much stronger westerly flow (negative values of stream function in the dark blue shading) that penetrates deep into northern tropics in the western hemisphere and "consumes" the NASM anticyclone in the "$4 \times CO_2$ world" (note that in the $4 \times CO_2$ simulations, there is no longer an anticyclone over North America). These changes in the stream function above the Pacific and North American regions are depicted in Figure 1c as negative differences relative to the control simulations.

Although outside of the main scope of this paper, Figure 1 also shows important changes in the circulations near the equator and in the tropics of the southern hemisphere. The anticyclone that forms over the Indian ocean south of equator is much stronger in the $4 \times CO_2$, simulations, which is also a robust response across models. As we will show in the next section of this paper, the increasing strength of the Indian Ocean UTLS anticyclone is a response to increased sea surface temperatures. Furthermore, a cross-equatorial southward flow above the Indian Ocean that connects the ASM anticyclone to the Indian ocean anticyclone in the southern hemisphere also intensifies in the $4 \times CO_2$ experiments. Using idealized tracers, Orbe et al. (2016) and G. Chen et al. (2017) showed that the ASM plays a key role in the cross-equatorial flow above 200 hPa during boreal summer. Since meridional tracer transport is partially determined by the strength of the meridional winds, interhemispheric transport of chemical constituents and aerosols in the UTLS is also expected to become stronger due to an increase in the GHGs. This argument is in agreement with the increase in the idealized tracer (i.e., a tracer that is emitted over the NH midlatitude surface) between 0 -10°S over the Indian Ocean due to quadrupled CO_2 from one of the CMIP6 models (GISS), indicating enhanced interhemispheric transport (not shown). The responses of the interhemispheric transport and the Indian Ocean anticyclone to increased levels of GHGs are subjects of future detailed investigation.

The circulation above Asia and North America, where anticyclones persist during NH summer, undergoes a strong seasonal cycle. Figure 3a shows the seasonal variations in the stream function from 11 Control (in red) and $4 \times CO_2$ (in black) simulations, averaged over the area of the ASM anticyclone (20°N–40°N and 40°E–100°E) at 100 hPa. The seasonal cycle amplitude (i.e., the difference between maximum and minimum in the area-averaged stream function during the climatological year) is larger in the $4 \times CO_2$ than Control simulations. This is mostly due to more negative stream function (stronger westerly flow) during NH winter and spring in the $4 \times CO_2$ experiments. In July and August, the coupled models produce smaller differences in the strength of the stream function above Asia than during boreal winter. The multi-model average over July-August from $4 \times CO_2$ simulations (thick black line) is slightly smaller than from control simulations (thick red line). Thus, the enclosed anticyclone above Asia forms later and more rapidly under $4 \times CO_2$ conditions, as it develops to its full strength. Increase in the seasonal cycle amplitude also suggests that more energy is available under the $4 \times CO_2$ conditions for formation and maintaining ASM anticyclone (see Section 6 for more discussion).

Regional differences in the seasonal strength of the UTLS circulation are further examined in Figure 4. The seasonal strength in the Control (Figure 4a) and $4 \times CO_2$ (Figure 4b) runs are shown as a difference between stream function averaged during July - August (i.e., peak in the strength of the UTLS anticyclones) and April - May (i.e., pre-monsoonal flow) at 100 hPa above Asia and North America. Figure 4c indicates that

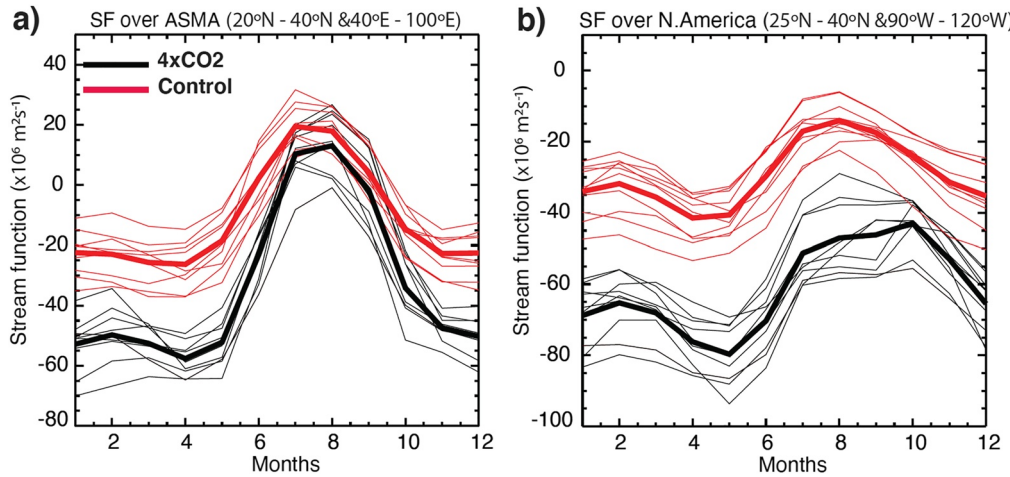

Figure 3. Seasonality of the stream function (in $\times 10^6$ m^2s^{-1}), averaged over the area of (a) the Asian Summer monsoon anticyclone (20°N–40°N and 40°E–100°E) and (b) North American summer Monsoon Anticyclone (25°N–40°N and 90°W–120°W) at 100 hPa. Red lines show climatological values from control simulations, while black lines show last 50-year averages (100-150-years) from 4 × CO_2 simulations. Thick lines are multi-model average.

quadrupled CO_2 leads to the seasonal intensification of the ASM anticyclone in the NH (positive contours) and the Indian ocean anticyclone in the SH (negative contours).

Changes in the seasonal cycle amplitude of the 100 hPa circulation above the NASM due to quadrupled CO_2 are much smaller than above Asia, see Figures 3b and 4. The stream function averaged over the NASM region (25°N–40°N and 90°W–120°W) is consistently more westerly in the "4 × CO_2 world" than in the Control simulations throughout the year (Figure 3b). Figure 4c also shows a small difference between seasonal strengths of the circulation in the Control and 4 × CO_2 simulations in the western hemisphere. Stronger westerly flow in the 4 × CO_2 runs during July-August, shown in Figure 3b, is in agreement with the stronger westerly jet that meanders deep into the northern tropics in the western hemisphere.

Acceleration and equatorward expansion of the westerly jet in the western hemisphere due to increased levels of CO_2 are also clearly seen in the vertical profile of the zonal wind differences between Control and 4 × CO_2 simulations, averaged over the 11 coupled models (Figure 5). There are positive anomalies on the upper flank of the NH subtropical jet (between 15°N– 30°N and 200 -70 hPa) that are consistent across all models (shown by hatching in Figure 5; also see Figure S2 in the Supporting Information S1 for zonal wind responses from individual models). The strengthening and equatorward expansion of the zonal-mean subtropical upper tropospheric westerly jet is a very robust result in models and is closely connected to the enhanced warming in tropical upper troposphere (Li et al., 2009, 2010; McLandress & Shepherd, 2009; Menzel et al., 2019). Previous studies of the upper tropospheric jets showed a close connection between variability of the subtropical westerly jet and the upper level anticyclones (Manney & Hegglin, 2018; Manney

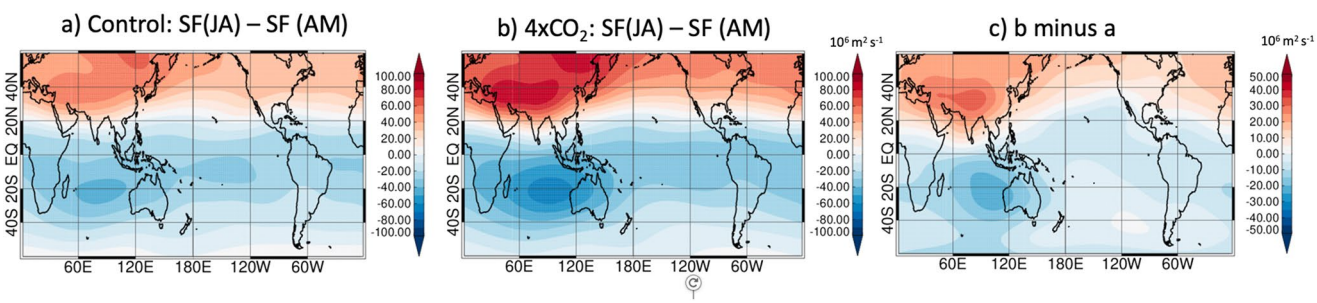

Figure 4. Differences in the 100 hPa stream function averaged between July-August and April-May from the (a) Control and (b) last fifty years of 4 × CO_2 simulations. The difference between two ("b) minus (a)") is shown in (c) representing regionally resolved differences in seasonality due to quadrupled CO_2. Note that color bar for panel (c) is different from (a) and (b).

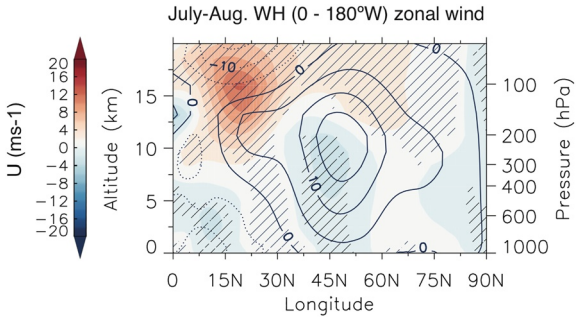

Figure 5. Latitude - height variations in the July-August zonal wind differences between the last 50-years of the $4 \times CO_2$ and Control ($4 \times CO_2$ – Control) simulations (in shading), averaged over the western hemisphere and 11 coupled models. Black contours correspond to zonal winds from the Control simulations with westerlies and easterlies shown as solid and dashed contours respectively. Hatching indicates regions where at least 9 out of 11 models agree on the sign of change.

et al., 2014, 2021; Schiemann et al., 2009). Our study also shows that quadrupling of the CO_2 in coupled models leads to an equatorward shift of the ASM anticyclone, which is in agreement with a recent study by Manney et al. (2021), showing a strong positive correlation in the location between the anticyclone and subtropical westerly jet. Yet, the cause and effect remains unclear and is a subject of future investigations.

Almost all general circulation and chemistry-climate models (including model simulations used in this study) predict a robust upward displacement of the tropopause height in the warming climate (Gettelman et al., 2010; Kim et al., 2013). Thus, it is reasonable to wonder whether the upper-level monsoon anticyclones shift together with the tropopause. Unfortunately, the detailed analysis of the vertical structure of the UTLS anticyclones requires a higher vertical resolution of outputs than CMIP6 currently provides us (archived pressure levels above and below 100 hPa are 70 and 150 hPa respectively). The circulation response to $4 \times CO_2$ at 70 hPa (not shown) is in qualitative agreement with the response at 100 hPa (e.g., smaller stream function differences in July-August above Asia than North America). However, there is a larger inter-model spread since the UTLS anticyclones start to weaken at this height, which is model-dependent. Furthermore, the NASM anticyclone is significantly weaker but still present at 70 hPa, suggesting the formation of the NASM anticyclone at much higher levels in the $4 \times CO_2$ simulations. Nevertheless, the unchanged sign of the circulation response throughout the vertical range doesn't suggest a vertical shift of the anticyclone. A full explanation of this question requires a more detailed analysis with a higher vertical resolution of outputs.

4. The Direct Radiative Effect of CO_2 vs Indirect SST Warming

The summertime UTLS circulation response to the quadrupled CO_2 in the coupled models can be decomposed into components associated with direct radiative forcing (fast adjustment) and indirect SST warming (slow adjustment) using idealized experiments from atmosphere-only GCMs with prescribed SSTs and CO_2 concentrations (see Section 2.2). Although prescribing SSTs to the GCM prevents some feedbacks between the ocean and atmosphere, this has very little influence on the large-scale UTLS circulation (e.g., the differences in the UTLS stream function between coupled ocean–atmosphere and atmosphere-only models with the same forcings are very small (not shown)).

We first examine the ASM anticyclone's response to prescribed forcings. Figure 6 shows climatological averages of 100 hPa stream function and horizontal winds in July and August from experiments conducted using atmosphere-only version of the CNRM-CM6 model. The circulation above Asia in the model experiment with prescribed preindustrial SSTs and GHGs (Figure 6a) is significantly stronger than in the simulation with $4 \times CO_2$ and SSTs taken from the end of the coupled model $4 \times CO_2$ run (i.e., "both forcings", Figure 6b). The stream function in the simulation with $4 \times CO_2$ but without SST warming (Figure 6c) is very similar to one with the preindustrial conditions (Figure 6a). In contrast, the simulation that is forced with warmer SSTs while keeping preindustrial levels of CO_2 shows a substantial (and statistically significant) weakening of the ASM anticyclone (Figure 6d) and very similar to the "both forcings" scenario. Thus, the response of the UTLS circulation above Asia is dominated by the impact of indirect SST warming. These results are consistent across three different models with the same set of idealized experiments (readers are referred to the supplemental materials showing the same figure for CESM2 and HadGem3).

Statistical characteristics reflecting the strength and location of the ASM anticyclone in the idealized experiments from three atmosphere-only models are summarized in Figures 7a and 7b respectively. We also show the $4 \times CO_2$ and Control experiments from corresponding coupled models to demonstrate small and insignificant differences in the strength and location of the ASM anticylone between the coupled $4 \times CO_2$ (Control) and the prescribed aSSTice+$4 \times CO_2$ (piSSTice) simulations. In comparison to the simulations with prescribed preindustrial conditions (piSSTice), simulations with SST warming-only forcing (a4SSTice)

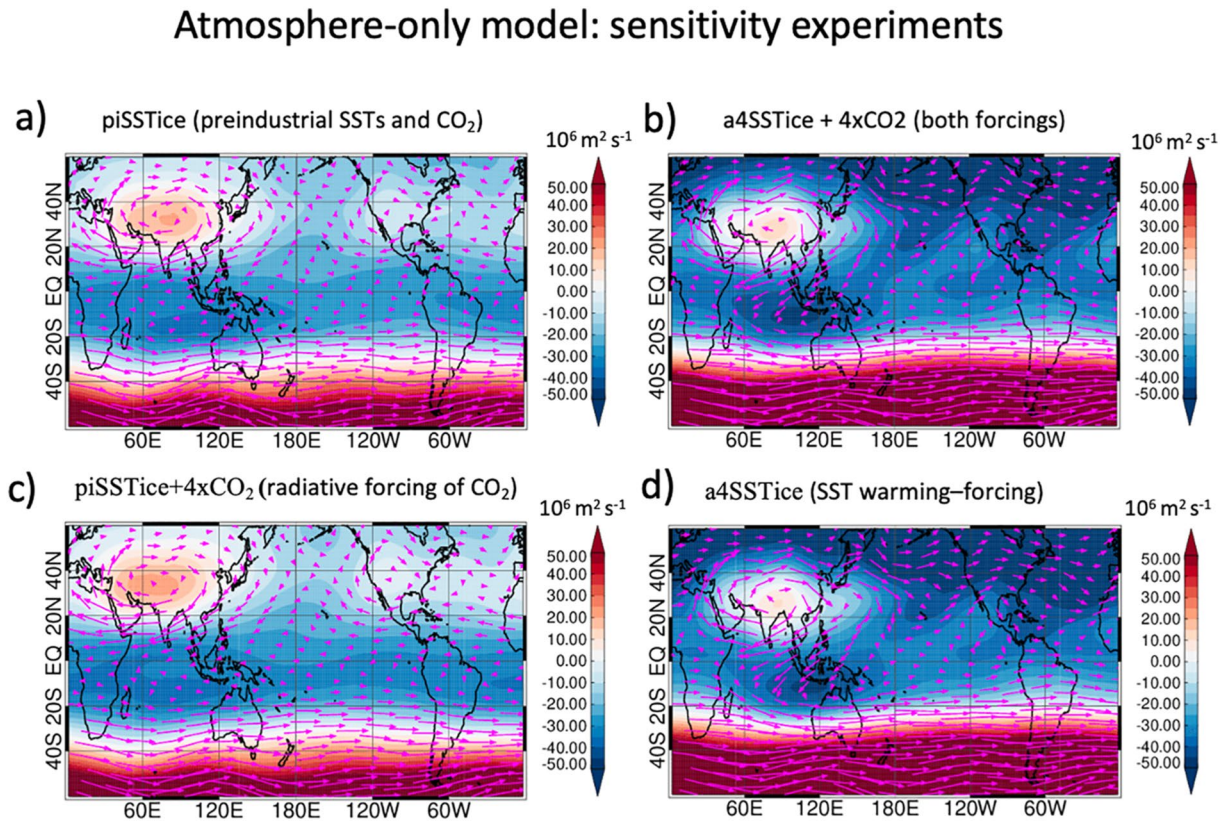

Figure 6. Stream function (shaded) and horizontal winds (arrows) at 100 hPa during July-August from CNRM-CM6 simulations with prescribed SSTs and CO_2: (a) preindustrial SSTs and CO_2 (piSSTice), (b) warmer SSTs, taken from the end of $4 \times CO_2$ coupled model run, and $4 \times CO_2$ (a4SSTice+$4 \times CO_2$), (c) preindustrial SSTs and quadrupled CO_2 (piSSTice +$4 \times CO_2$), (d) preindustrial CO_2 and warmer SSTs from the end of $4 \times CO_2$ couple model experiment (a4SSTice).

produce a significantly weaker area-averaged stream function above Asia (Figure 7a). On the other hand, the ASM anticyclone either becomes stronger (for HadGEM3 and CESM2, statistically significant) or remains nearly the same (for CNRM, not statistically significant) with direct radiative effect of $4 \times CO_2$-only forcing (piSSTice+$4 \times CO_2$) when compared to the preindustrial conditions (piSSTice). As a consequence, imposing both warmer SSTs and $4 \times CO_2$ forcings results in an anticyclone that is weaker than in the preindustrial Control but stronger than in the SST warming-only simulations.

Figure 7b shows the differences in the latitude of the ASM anticyclone's center due to different forcings. The radiative effect of $4 \times CO_2$- and SST warming-only forcings result in northward and southward shifts of the ASM anticyclone respectively with a larger magnitude of the equatorward than southward shift. The combined, a4SSTice+$4 \times CO_2$, response is dominated by the SST feedback, leading to a significant equatorward shift of the anticyclone in the total response.

Idealized experiments with atmosphere-only GCMs also show the dominant role of the SST warming on the circulation changes in the western hemisphere. Figure 6c indicates that the NASM anticyclone remains unchanged under direct radiative forcing of $4 \times CO_2$. The response of the 100 hPa stream function is heavily dominated by the SST feedback, resulting in a stronger westerly flow that penetrates deep into the northern tropics and consumes the NASM anticyclone (Figure 6d). This is in agreement with Figure 8 showing the response of the western hemisphere zonal wind to idealized forcings during July-August. Positive western hemisphere zonal wind anomalies on the upper and equatorward flank of the subtropical jet from SST warming-only forcing (Figure 8b) are similar in the location and magnitude to anomalies from all-forcing simulations (Figure 8a), while $4 \times CO_2$-only forcing has very little impact on the western hemisphere zonal flow (Figure 8c).

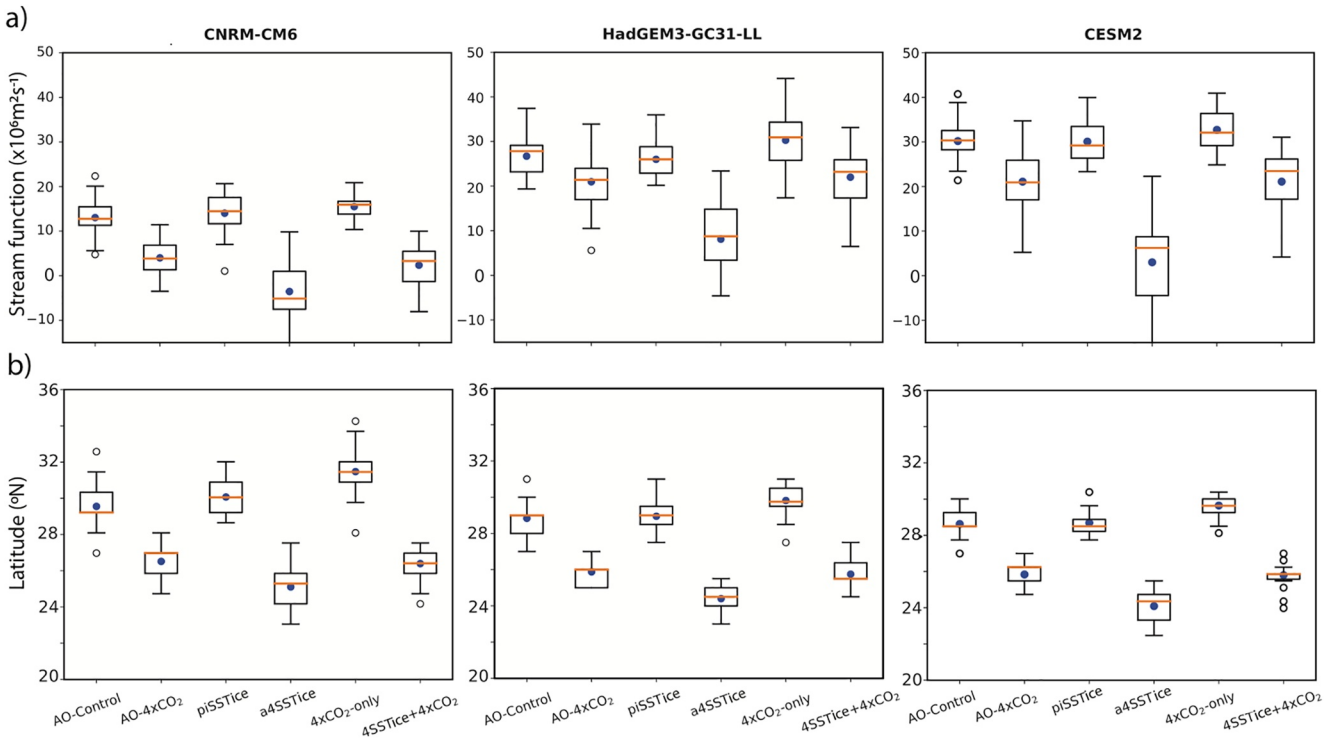

Figure 7. (a) 100 hPa stream function in July-August, averaged over the area of ASM anticyclone (20°N–40°N and 40°E–100°E); (b) latitude of maximum in 100 hPa stream function above Asia in July-August from the coupled atmosphere-ocean (AO) and idealized GCM experiments (left to right: Control, 4 × CO_2, piSSTice, a4SSTice, 4 × CO_2-only, and a4SSTice+4 × CO_2). Shown are median (horizontal line), mean (blue dot), 25th - 75th percentiles (box), minimum and maximum values (whiskers), and outliers (dots).

While lower tropospheric circulation show very distinct compensation effects over the most regions in the NH (Shaw & Voigt, 2015), our study shows a dominant effect of the SST warming on the monsoon anticyclones in the UTLS. Thus, the mechanisms solely based on the land-ocean temperature contrasts do not provides us with a full explanation of why coupled models produce smaller changes in the strength of the ASM anticyclone in comparison to the response over North America.

A possible contributor to the differences in the UTLS anticyclone responses between the Asian and North American monsoons could be regional changes in the convective heating. Both Asian and North American UTLS anticyclones are thought to arise primarily as a response to diabatic heating associated with land-ocean contrasts and convection near the Tibetan/Iranian and Colorado plateaus respectively (Garny & Randel, 2013; Hoskins & Rodwell, 1995; Liu et al., 2004, 2007; Ren et al., 2019; Yongfu et al., 2002, and references therein). While land-ocean temperature contrasts are fundamental for the formation of monsoons, a significant part of total diabatic heating comes from the latent heat of condensation released by tropical and subtropical precipitation (Gill, 1980; Hoskins & Rodwell, 1995; Phlips & Gill, 1987; Webster, 1972). In particular, Siu and Bowman (2019) investigated the forcing mechanisms of the NASM anticyclone using a simplified dry general circulation model. They showed that the ASM anticyclone is stronger than the NASM anticyclone, primarily because precipitation in the subtropics over Asia is much larger than at similar latitudes in the Western Hemisphere. They also demonstrated that the NASM anticyclone is primarily a response to heating poleward of 15°N, which includes the northern part of Central America, Mexico, the southern United States, the Caribbean Sea, and the Gulf of Mexico. Thus, regional changes in the latent heat of condensation released by extratropical precipitation in the warming climate could potentially explain the differences in the observed responses of the UTLS anticyclones.

Quadrupling CO_2 without increase in the SSTs typically generates warming of the surface, which leads to increased land-ocean temperature contrast. Increase in the land-ocean temperature contrast would generate an intensification of the UTLS anticyclones. When the SSTs increase, the land-ocean temperature

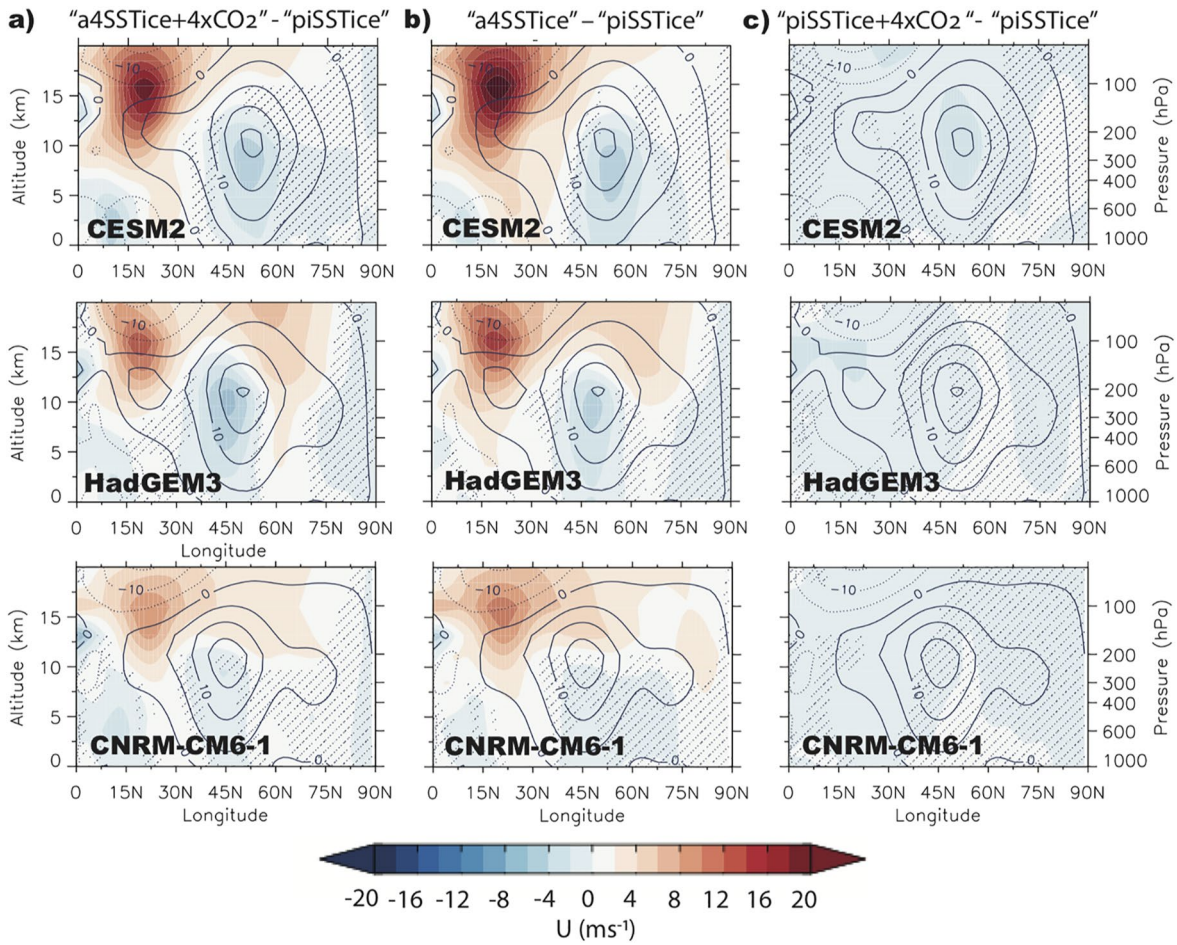

Figure 8. Latitude - height variations in a response of July-August zonal winds (color shading), averaged over the western hemisphere, relative to the preindustrial conditions (piSSTice, shown in contours) from thee atmosphere-only GCMs (from top to bottom: CESM2, HadGEM3-GC31-LL, and CNRM-CM6-1). Shown are differences in zonal winds due to: (a) both forcings ("a4SSTice+ 4 × CO_2" – "piSSTice"); SSTs-only forcing ("a4SSTice" – "piSSTice"); (c) 4 × CO_2-only forcing ("piSSTice+4 × CO_2" – "piSSTice"). Contour intervals are every 2 m s^{-1}. Stippling indicates differences that are not statistically significant at the 95 percent confidence level based on a Student's t-test.

contrast is greatly reduced and the monsoon circulation is weaker. However, our results show bigger differences in the seasonality of the response to 4 × CO_2 above Asia than North America in Figures 3 and 4. An increase in convective heating above Asia, could add enough energy to the system for the monsoon development. We confirmed that the precipitation rates, a proxy for the convective activity, above Asia in the 4 × CO_2 simulations for the 6 models increase (this field is not included in the CMIP6 archive for all models; see Figure S4 in Supporting Information S1), which is also in agreement with other studies investigating the impact of GHG increase on the boreal summer precipitation (Z. Chen et al., 2020; Li & Ting, 2017). In contrast, precipitation rates poleward of 10°N decrease over North America. A strong drying trend in the western United States from the simulations with combined as well as coupled forcings was documented by Li and Ting (2017), who examined future precipitation projections using CMIP5 models and attributed projected changes to the SST warming. Z. Chen et al. (2020) showed that the increase in precipitation above Asia in CMIP6 models are dominated by the increase in atmospheric moisture under global warming, while a decrease in precipitation above the North American monsoon region is due to the effects of circulation changes. This proposed (or other possible) mechanisms of the UTLS response to the quadrupled CO_2 needs to be further investigated and tested in future modeling studies.

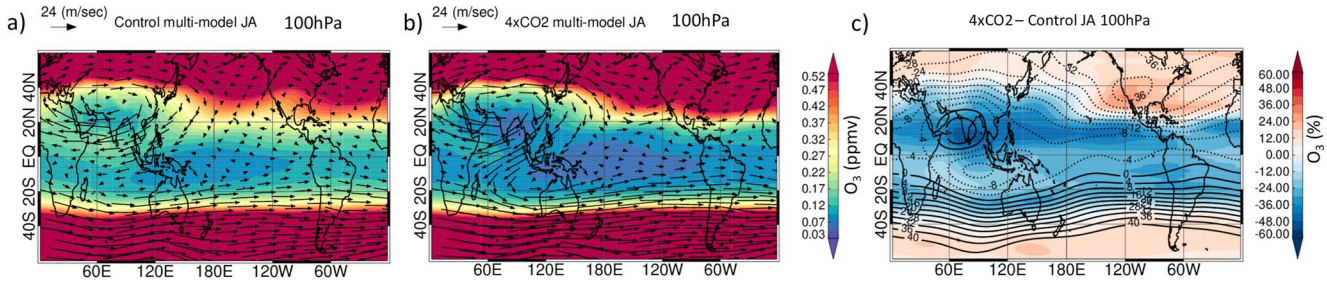

Figure 9. July-August ozone (shaded, in ppmv) and wind vectors at 100 hPa averaged over nine GCMs with coupled ocean–atmosphere for (a) climatological average of the Control simulations, and (b) 100 - 150-year average of perturbed $4 \times CO_2$ simulations. Reference wind vector is 24 m s^{-1} (c) Ozone (shaded, in % relative to Control simulations) and stream function (contours, in $\times 10^6$ m^2 s^{-1}) differences, $4 \times CO_2$ – Control simulations.

5. Response of Ozone to Changes in Circulation Due to Quadrupled CO_2

Ozone changes in the UTLS are driven primarily by the circulation acting on the strong background horizontal and vertical gradients because at these levels ozone's lifetime is long so its distribution is mostly controlled by dynamics. Previous studies showed that strengthening (weakening) of the ASM anticyclone can lead to stronger (weaker) ozone transport from extratropics deep into the northern tropics (Das et al., 2019; Tweedy et al., 2018; Yan et al., 2018). At the same time, a change in the location of the anticyclone itself would result in the displacement of low ozone that is trapped inside the circulation. Thus, it is important to examine and quantify ozone and other trace gas response to the anomalous changes in the circulation due to increases in CO_2. Here we examine the changes in the ozone field to highlight changes in the tropical and extratropical UTLS composition. (Note, that there are only limited chemical constituents included in the CMIP6 archive, and fields of tracers, like CO, that are often used to track motion in the monsoons are not available.)

We first examine the climatological 100 hPa multi-model mean ozone and horizontal winds in July-August for the Control experiments. Figure 9a shows that ASM anticyclone provides the most distinct nonzonal feature in ozone with a region of low mixing ratios trapped inside the circulation cell (centered at 20°N over the Indian subcontinent) and a band of higher ozone that penetrates from the extratropical Pacific into the northern tropics. These climatological features of ozone distribution associated with the ASM anticyclone have been well documented (Konopka et al., 2010; Park et al., 2007; Randel & Park, 2006).

In $4 \times CO_2$ simulations (Figure 9b), ozone values decrease across the tropics and increase across the higher latitudes. These ozone changes are highlighted in Figure 8c, showing ozone differences relative to the Control simulations, and connected by previous studies to the changes in the large-scale vertical transport (Chiodo et al., 2018; Li et al., 2009; Shepherd, 2008). For instance, the decrease in the UTLS tropics-wide ozone due to stronger tropical upwelling was examined by Chiodo et al. (2018) and Chiodo et al. (2021) using similar model simulations from CMIP5 and CMIP6. Acceleration of the advective components of the Brewer-Dobson circulation (e.g., upwelling in the tropics and downwelling in the extratropics) due to increase in CO_2 is one of the most robust responses amongst the models (Rind et al., 1998, 2002; Butchart & Scaife, 2001; Butchart et al., 2010; Garcia & Randel, 2008; Hardiman et al., 2014; Li et al., 2008; Oberländer et al., 2013; Sigmond et al., 2004). Enhanced tropical upwelling leads to the ozone decrease by bringing loW–ozone tropospheric air to the tropical UTLS, while enhanced downwelling in the extratropics leads to the increase in ozone by transporting ozone-rich air from the stratosphere to the extratropical UTLS.

Superimposed on the global ozone anomalies are very strong regional ozone differences in the NH. Negative ozone anomalies are greatest above the northern tropics Indian Ocean, the northern tropical Pacific, and the ASM anticyclone's southeast edges. These anomalies are in agreement with changes in stream function at 100 hPa (black contours in Figure 9c). Positive stream function anomalies over the northern Indian ocean coincide with pronounced reduction in ozone. Thus, as ASM anticyclone shifts equatorward, so does low ozone trapped inside of it, resulting in less ozone in the northern tropical Indian Ocean. Ozone reduction at the ASM anticyclone's southeast edges could be by increased upwelling or/and reduced trapping by the weaker ASM anticyclone. The meandering of the subtropical jet deep into the tropics leads to horizontal

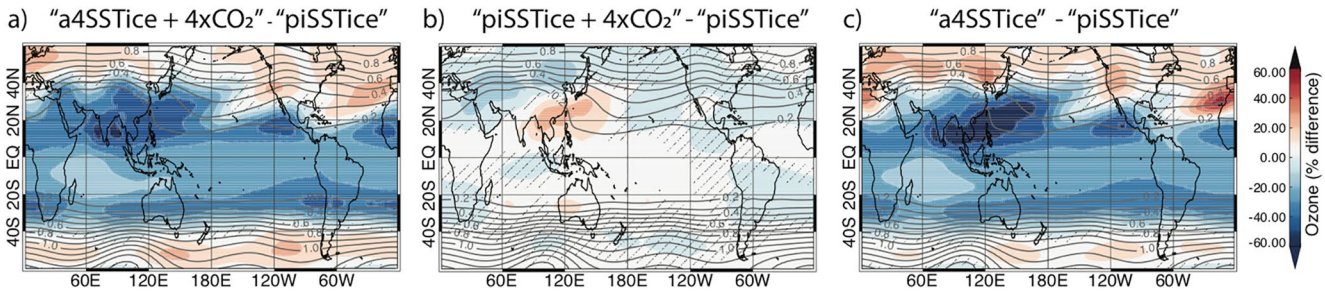

Figure 10. Ozone response to the prescribed SST and CO_2 forcings in July-August at 100 hPa from CNRM-CM6 . Ozone differences (shaded) are shown as percentages relative to the preindustrial conditions (piSSTice, gray contours) due to (a) both forcings (a4SSTice+4 × CO_2); (b) quadruped CO_2 (piSSTice+ 4 × CO_2); (c) warmer SSTs from the end of the coupled model 4 × CO_2 simulation (a4SSTice). Stippling indicates differences that are not statistically significant at the 95 percent confidence level based on a Student's t-test.

transport of high ozone from the extratropics deep into the western hemisphere tropics (especially above North America). Furthermore, ozone decreases inside the ASM anticyclone and throughout northern tropical western pacific in the 4 × CO_2 simulations (Figure 9b), possibly due to enhanced upwelling (not shown). The ozone response to the 4 × CO_2 is robust across 9 models and interested readers are referred to Figure S5 in Supporting Information S1, which shows ozone differences in individual models.

Comparison of the coupled 4 × CO_2 simulations with those using prescribe SST and CO_2 forcings indicate the extent to which 100 hPa ozone changes reflect rapid and fast adjustments (Figure 10). The tropics-wide ozone decrease in "both forcing" simulations (Figure 10a), associated with acceleration of tropical upwelling, is dominated by the indirect SST warming (Figure 10c). Direct radiative effect of CO_2 produces very small (and for many regions insignificant) changes in the tropical ozone (Figure 10b) while simulations with SST-only forcing result in ozone changes similar to those with both, 4 × CO_2 and SST warming, forcings. These results are in agreement with (Orbe et al., 2020) and (Oman et al., 2009), who showed that the response in the lower stratospheric upwelling is dominated by feedbacks associated with changes in SSTs.

The ozone response to the individual SST and CO_2 forcings (Figure 10) relative to the preindustrial Control also reflects differences in the strength and location of the ASM anticyclone. 4 × CO_2-only forcing results in a small (but statistically significant) positive ozone anomaly along the coast of southeast Asia (Figure 10c), which is due to a slightly stronger ASM circulation (compare stream function maps between Figures 6a and 6c). The response of ozone to the SST-only forcing is much greater, and reflects the significantly weaker ASM anticyclone and its equatorward shift. For instance, negative ozone anomalies above northern tropical Indian ocean are co-located with positive stream function anomalies, indicative of the shift in the ASM anticyclone. At the same time, large negative anomalies along South East Asia are in agreement with a significantly weaker ASM anticyclone, which brings less ozone into the tropics. When both SST and CO_2 forcings are prescribed, there is some cancellation in the total response, but the ozone response to the SST adjustment generally dominates the direct 4 × CO_2 feedback .

To summarize, we identified several effects leading to ozone decrease in the 4 × CO_2 simulations (seen in Figure 9c) due to: (a) enhanced tropics-wide upwelling; (b) southward shift in the ASM anticyclone over the northern tropical Indian ocean; (c) reduced trapping and/or horizontal advection of ozone along South East Asia, associated with the weaker ASM anticyclone; and (c) likely enhanced vertical transport within the ASM anticyclone. Figure 10 shows that most of these changes are due to SST warming, consistent with previous figures. Still, full separation and relative contributions of the ozone reduction mechanisms would require a detailed evaluation of regional ozone and other trace gases (e.g., CO) transport budget, which is left for future modeling investigations.

6. Discussions and Conclusions

In this study, we examined the response of the northern hemisphere summer monsoon anticyclones and ozone to the abrupt quadrupling of CO_2 using monthly outputs from coupled ocean–atmosphere general circulation models. We have shown that 4 × CO_2 in the coupled atmosphere ocean models result in:

1. An equatorward shift of the ASM anticyclone;
2. A small decrease in the strength of the ASM anticyclone during July and August;
3. The disappearance of the NASM anticyclone at 100 hPa with stronger and more equator-ward westerly flow in the western hemisphere throughout the year;
4. An increase in the seasonal amplitude of the circulation above Asia due to more westerly flow during boreal winter and spring.

Three CMIP6 atmosphere-only general circulation models with prescribed SSTs and sea ice concentration were used to isolate the direct atmospheric radiative effect of CO_2 from indirect SST warming. It was also shown that SST-only forcing heavily dominates $4 \times CO_2$-only forcing in producing a southward displacement and a larger seasonal strength of the ASM anticyclone, a disappearance of the NASM anticyclone, and a strengthening upper-level subtropical westerly jet in the western hemisphere. We suggest an important role of regional changes in convective activity (and associated with it latent heat of condensation) in the warmer SST settings. This study showed that the ASM anticyclone strength in July and August either slightly weakens or doesn't change significantly due to quadrupled CO_2 in coupled models, but its seasonal strength becomes larger. Increased latent heating released by increased precipitation over Asia could provide enough energy for development of the ASM anticyclone and offset the expected weakening of the monsoon system due to reduced land-ocean temperature gradients. Contrarily, the precipitation rates (and thus convective activity) are reduced over the NASM anticyclone, resulting in a very robust weakening of the anticyclone. This proposed mechanism of documented changes in UTLS anticyclones yet needs to be tested in future investigations.

Changes in the ASM and NASM anticyclones due to quadrupled CO_2 result in:

1. A significant impact on the tropical and extratropical distribution of the NH ozone in the UTLS with a decrease in ozone greater than 40%–50% relative to the Control above the NH tropical Indian Ocean, Western Pacific and central Pacific.
2. Higher ozone anomalies between 20°N–30°N in the Eastern Pacific and North America due to the disappearance of the NASM anticyclone

The response of ozone to individual forcing based on monthly output from one model is in agreement with changes in the strength of the circulation. Strengthening/weakening of the ASM anticyclone leads to positive/negative ozone anomalies along the coast of South East Asia in the simulation with $4 \times CO_2$/SST-only forcing. Ozone response to the $4 \times CO_2$ partially offsets the response to warming SSTs.

The ozone response to $4 \times CO_2$ in the coupled models strongly resembles that due to ENSO events in (Tweedy et al., 2018) study. They showed strong negative/positive ozone sensitivities in the NT during boreal summer due to El Nino/La Nina events. This is not a surprise since in both studies SSTs are involved in modulating the strength of the ASM anticyclone. During El Nino/La Nina, the SSTs in the equatorial Pacific are anomalously high/low, leading to a negative/positive land-sea temperature contrast and weaker/stronger ASM anticyclone. This indicates the important role of the SSTs for both interannual variability and future changes of UTLS summertime ozone.

The circulation changes due to an increased level of CO_2 has a significant impact on boreal summer UTLS ozone, that could further change climate; however, most models in CMIP6 have prescribed stratospheric ozone, and are therefore missing the ozone radiative feedback. A lack of interactive ozone and its feedbacks on temperature and water vapor near the tropopause could add additional uncertainty in the future predictions of climate (Nowack et al., 2015).

Although very simple and exaggerated, the abrupt $4 \times CO_2$ forcing simulations allowed for a mechanistic look into the response characteristics of GCMs that can be unambiguously attributed to an increase in CO_2 concentrations. Initial analysis of model simulations with more realistic climate change scenarios shows very similarly (only weaker in magnitude) changes in the UTLS boreal summer circulation, including an equatorward shift in the ASM anticyclone and intensification of the subtropical westerly jet above the Pacific and North America. The impact of these changes on chemical composition is a topic of future detailed investigation using climate change simulations from chemistry-climate models.

The results of our multi-model analysis also indicate a strong potential for intensification of the inter-hemispheric transport (IHT) during boreal summer in the narrow region over the Indian Ocean due to an increase in GHGs. IHT is a key process affecting global redistribution of atmospheric air pollutants and greenhouses gases (Hartley & Black, 1995; Newell et al., 1974; Staudt et al., 2001; Wang & Shallcross, 2000). Orbe et al. (2016) and G. Chen et al. (2017) showed that the boreal summer interhemispheric transport over Indian Ocean is connected to the advection by the strong cross-equatorial winds at the southward edge of the Asian monsoon anticyclone. This study has shown that cross-equatorial flow above the Indian Ocean in the abrupt $4 \times CO_2$ simulations becomes stronger. Furthermore, a southward shift in the ASM anticyclone displaces regions of strong horizontal ozone gradients, equatorward. Stronger meridional winds and horizontal tracer gradients are both favorable conditions for the ITH intensification. Improved understanding of the IHT and its underlying mechanisms is necessary for the quantification of sources and sinks of pollutants and the estimation of their potential to affect the global climate, especially in light of projected anthropogenic climate change.

Data Availability Statement

GEOSCCM simulations are stored in their data-storage facility and the data, used for this study, are available for download at NASA's Open Data Portal (https://doi.org/10.25966/8st2-jz22).

Acknowledgments
O. V. Tweedy was supported by an appointment to the NASA Postdoctoral Program at the NASA's Goddard Space Flight Center, administered by Universities Space Research Association under contract with NASA. F. Li acknowledges the GEOSCCM simulations were funded by NASA's Atmospheric Composition Modeling and Analysis Program (ACMAP) under Grant NNX17AF62G. CMIP6 DECK simulations discussed in this study are available through the Earth System Grid Federation (ESGF; https://esgf-node.llnl.gov/search/cmip6/). The GEOSCCM is supported by the NASA Modeling, Analysis, and Prediction (MAP) program and by the Center for Climate Simulation (NCCS). The authors would like to acknowledge John Kummer for helpful discussion and comments of this work. The authos thank the three reviewers for their substantive comments, which helped to improve the manuscript.

References

Abalos, M., Randel, W. J., Kinnison, D. E., & Garcia, R. R. (2017). Using the artificial tracer e90 to examine present and future UTLS tracer transport in WACCM. *Journal of the Atmospheric Sciences*, *74*(10), 3383–3403. https://doi.org/10.1175/JAS-D-17-0135.1

Bader, D. C., Leung, R., Taylor, M., & McCoy, R. B. (2019a). *E3SM-Project E3SM1.0 model output prepared for CMIP6 CMIP abrupt-4xCO2*. https://doi.org/10.22033/ESGF/CMIP6.4491

Bader, D. C., Leung, R., Taylor, M., & McCoy, R. B. (2019b). *E3SM-Project E3SM1.0 model output prepared for CMIP6 CMIP piControl*. https://doi.org/10.22033/ESGF/CMIP6.4499

Basha, G., Ratnam, M. V., & Kishore, P. (2020). Asian summer monsoon anticyclone: Trends and variability. *Atmospheric Chemistry and Physics*, *20*(11), 6789–6801. https://doi.org/10.5194/acp-20-6789-2020

Bony, S., Bellon, G., Klocke, D., Sherwood, S., Fermepin, S., & Denvil, S. (2013). Robust direct effect of carbon dioxide on tropical circulation and regional precipitation. *Nature Geoscience*, *6*(6), 447–451. https://doi.org/10.1038/ngeo1799

Butchart, N., Cionni, I., Eyring, V., Shepherd, T. G., Waugh, D. W., Akiyoshi, H., & Tian, W. (2010). Chemistry–climate model simulations of twenty-first century stratospheric climate and circulation changes. *Journal of Climate*, *23*(20), 5349–5374. https://doi.org/10.1175/2010JCLI3404.1

Butchart, N., & Scaife, A. A. (2001). Removal of chlorofluorocarbons by increased mass exchange between the stratosphere and troposphere in a changing climate. *Nature*, *410*(6830), 799–802. https://doi.org/10.1038/35071047

Chen. (2003). Maintenance of summer monsoon circulations: A planetary-scale perspective. *Journal of Climate*, *16*(12), 2022–2037. https://doi.org/10.1175/1520-0442(2003)016<2022:mosmca>2.0.co;2

Chen, G., Orbe, C., & Waugh, D. (2017). The role of monsooN–like zonally asymmetric heating in interhemispheric transport. *Journal of Geophysical Research: Atmospheres*, *122*, 3282–3298. https://doi.org/10.1002/2016JD026427

Chen, Z., Zhou, T., Zhang, L., Chen, X., Zhang, W., & Jiang, J. (2020). Global Land Monsoon Precipitation Changes in CMIP6 Projections. *Geophysical Research Letters*, *47*. https://doi.org/10.1029/2019gl086902

Chiodo, G., Ball, W. T., Nowack, P., Orbe, C., Keeble, J., Diallo, M., & Hassler, B. (2021). The response of the ozone layer under abrupt $4xco_2$ in cmip6. *EGU General Assembly*, *2021*. https://doi.org/10.5194/egusphere-egu21-15283

Chiodo, G., Polvani, L. M., Marsh, D. R., Stenke, A., Ball, W., Rozanov, E., & Tsigaridis, K. (2018). The response of the ozone layer to quadrupled CO_2 concentrations. *Journal of Climate*, *31*(10), 3893–3907. https://doi.org/10.1175/JCLI-D-17-0492.1

Danabasoglu, G. (2019a). *NCAR CESM2-WACCM model output prepared for CMIP6 CMIP abrupt-4xCO$_2$*. https://doi.org/10.22033/ESGF/CMIP6.10039

Danabasoglu, G. (2019b). *NCAR CESM2-WACCM model output prepared for CMIP6 CMIP piControl*. https://doi.org/10.22033/ESGF/CMIP6.10094

Danabasoglu, G., Lawrence, D., Lindsay, K., Lipscomb, W., & Strand, G. (2019). *NCAR CESM2 model output prepared for CMIP6 CMIP piControl*. https://doi.org/10.22033/ESGF/CMIP6.7733

Das, S. S., Suneeth, K. V., Ratnam, M. V., Girach, I. A., & Das, S. K. (2019). Upper tropospheric ozone transport from the sub-tropics to tropics over the Indian region during Asian summer monsoon. *Climate Dynamics*, *52*(7–8), 4567–4581. https://doi.org/10.1007/s00382-018-4418-6

Dawson, A. (2016). Windspharm: A high-level library for global wind field computations using spherical harmonics. *Journal of Open Research Software*, *4*. https://doi.org/10.5334/jors.129

Douglas, M. W., Maddox, R. A., Howard, K., & Reyes, S. (1993). The Mexican Monsoon. *Journal of Climate*, *6*(8), 1665–1677. https://doi.org/10.1175/1520-0442(1993)006<1665:tmm>2.0.co;2

Dunkerton, T. J. (1995). *Stratosphere adjacent to monsoon regions stratosphere up to a maximum height* (p. 100).

Eyring, V., Bony, S., Meehl, G. A., Senior, C. A., Stevens, B., Stouffer, R. J., & Taylor, K. E. (2016). Overview of the coupled model intercomparison project phase 6 (cmip6) experimental design and organization. *Geoscientific Model Development*, *9*(5), 1937–1958. https://doi.org/10.5194/gmd-9-1937-2016

Garcia, R. R., & Randel, W. J. (2008). Acceleration of the brewer-dobson circulation due to increases in greenhouse gases. *Journal of the Atmospheric Sciences*, *65*(8), 2731–2739. https://doi.org/10.1175/2008JAS2712.1

Garny, H., & Randel, W. J. (2013). Dynamic variability of the Asian monsoon anticyclone observed in potential vorticity and correlations with tracer distributions. *Journal of Geophysical Research: Atmospheres*, *118*, 13421–13433. https://doi.org/10.1002/2013JD020908

Gettelman, A., Hegglin, M. I., Son, S.-W., Kim, J., Fujiwara, M., Birner, T., & Tian, W. (2010). Multimodel assessment of the upper troposphere and lower stratosphere: Tropics and global trends. *Journal of Geophysical Research*, *115*. https://doi.org/10.1029/2009JD013638

Gill, A. E. (1980). Some simple solutions for heat-induced tropical circulation. *Quarterly Journal of the Royal Meteorological Society*, *106*(449), 447–462. https://doi.org/10.1002/qj.49710644905

Hardiman, S. C., Butchart, N., & Calvo, N. (2014). The morphology of the Brewer-Dobson circulation and its response to climate change in CMIP5 simulations. *Quarterly Journal of the Royal Meteorological Society*, *140*(683), 1958–1965. https://doi.org/10.1002/qj.2258

Hartley, D. E., & Black, R. X. (1995). Mechanistic analysis of interhemispheric transport. *Geophysical Research Letters*, *22*(21), 2945–2948. https://doi.org/10.1029/95GL02823

Hoskins, B. J., & Rodwell, M. J. (1995). A Model of the Asian Summer Monsoon. Part I: The Global Scale. *Journal of the Atmospheric Sciences*, *52*(9), 1329–1340. https://doi.org/10.1175/1520-0469(1995)052<1329:AMOTAS>2.0.CO;2

Kamae, Y., Watanabe, M., Ogura, T., Yoshimori, M., & Shiogama, H. (2015). Rapid adjustments of cloud and hydrological cycle to increasing CO_2: A review. *Current climate change reports*, *1*(2), 103–113. https://doi.org/10.1007/s40641-015-0007-5

Kim, J., Grise, K. M., & Son, S.-W. (2013). Thermal characteristics of the cold-point tropopause region in cmip5 models. *Journal of Geophysical Research: Atmospheres*, *118*, 8827–8841. https://doi.org/10.1002/jgrd.50649

Konopka, P., Grooß, J.-U., Günther, G., Ploeger, F., Pommrich, R., Müller, R., & Livesey, N. (2010). Annual cycle of ozone at and above the tropical tropopause: Observations versus simulations with the Chemical Lagrangian Model of the Stratosphere (CLaMS). *Atmospheric Chemistry and Physics*, *10*(1), 121–132. https://doi.org/10.5194/acp-10-121-2010

Krasting, J. P., John, J. G., Blanton, C., McHugh, C., Nikonov, S., Radhakrishnan, A., & Zhao, M. (2018a). *NOAA-GFDL GFDL-ESM4 model output prepared for CMIP6 CMIP abrupt-4xCO$_2$*. https://doi.org/10.22033/ESGF/CMIP6.8489

Krasting, J. P., John, J. G., Blanton, C., McHugh, C., Nikonov, S., Radhakrishnan, A., & Zhao, M. (2018b). *NOAA-GFDL GFDL-ESM4 model output prepared for CMIP6 CMIP piControl*. https://doi.org/10.22033/ESGF/CMIP6.8669

Li, F., Austin, J., & Wilson, J. (2008). The strength of the brewer–dobson circulation in a changing climate: Coupled chemistry–climate model simulations. *Journal of Climate*, *21*(1), 40–57. https://doi.org/10.1175/2007JCLI1663.1

Li, F., & Newman, P. (2020). Stratospheric water vapor feedback and its climate impacts in the coupled atmosphere ocean Goddard Earth Observing System Chemistry-Climate Model. *Climate Dynamics*. https://doi.org/10.1007/s00382-020-05348-6

Li, F., Stolarski, R. S., & Newman, P. A. (2009). Stratospheric ozone in the post-cfc era. *Atmospheric Chemistry and Physics*, *9*(6), 2207–2213. https://doi.org/10.5194/acp-9-2207-2009

Li, F., Stolarski, R. S., Pawson, S., Newman, P. A., & Waugh, D. (2010). Narrowing of the upwelling branch of the Brewer-Dobson circulation and Hadley cell in chemistry-climate model simulations of the 21st century. *Geophysical Research Letters*, *37*. https://doi.org/10.1029/2010GL043718

Li, X., & Ting, M. (2017). Understanding the Asian summer monsoon response to greenhouse warming: The relative roles of direct radiative forcing and sea surface temperature change. *Climate Dynamics*, *49*(7–8), 2863–2880. https://doi.org/10.1007/s00382-016-3470-3

Liu, Y., Hoskins, B., & Blackburn, M. (2007). Impact of Tibetan orography and heating on the summer flow over Asia. *Journal of the Meteorological Society of Japan. Ser. II*, *85B*, 1–19. https://doi.org/10.2151/jmsj.85B.1

Liu, Y., Wu, G., & Ren, R. (2004). Relationship between the subtropical anticyclone and diabatic heating. *Journal of Climate*, *17*(4), 682–698. https://doi.org/10.1175/1520-0442(2004)017<0682:RBTSAA>2.0.CO;2

Ma, J., Xie, S. P., & Kosaka, Y. (2012). Mechanisms for tropical tropospheric circulation change in response to global warming. *Journal of Climate*, *25*(8), 2979–2994. https://doi.org/10.1175/JCLI-D-11-00048.1

Manney, G. L., & Hegglin, M. I. (2018). Seasonal and regional variations of long-term changes in upper-tropospheric jets from reanalyses. *Journal of Climate*, *31*(1), 423–448. https://doi.org/10.1175/JCLI-D-17-0303.1

Manney, G. L., Hegglin, M. I., Daffer, W. H., Schwartz, M. J., Santee, M. L., & Pawson, S. (2014). Climatology of upper tropospheric–lower stratospheric (UTLS) jets and tropopauses in MERRA. *Journal of Climate*, *27*(9), 3248–3271. https://doi.org/10.1175/JCLI-D-13-00243.1

Manney, G. L., Santee, M. L., Lawrence, Z. D., Wargan, K., & Schwartz, M. J. (2021). *A moments view of climatology and variability of the Asian summer monsoon anticyclone* (pp. 1–69). https://doi.org/10.1175/JCLI-D-20-0729.1

McLandress, C., & Shepherd, T. G. (2009). Simulated anthropogenic changes in the Brewer-Dobson circulation, including its extension to high latitudes. *Journal of Climate*, *22*(6), 1516–1540. https://doi.org/10.1175/2008jcli2679.1

Menzel, M. E., Waugh, D., & Grise, K. (2019). Disconnect between hadley cell and subtropical jet variability and response to increased CO_2. *Geophysical Research Letters*, *46*, 7045–7053. https://doi.org/10.1029/2019GL083345

NASA/GISS. (2018a). *NASA-GISS GISS-E2.1G model output prepared for CMIP6 CMIP abrupt-4xCO$_2$*. https://doi.org/10.22033/ESGF/CMIP6.6976

NASA/GISS. (2018b). *NASA-GISS GISS-E2.1G model output prepared for CMIP6 CMIP piControl*. https://doi.org/10.22033/ESGF/CMIP6.7380

Newell, R. E., Boer, G. J., & Kidson, J. W. (1974). An estimate of the interhemispheric transfer of carbon monoxide from tropical general circulation data. *Tellus*, *26*(1–2), 103–107. https://doi.org/10.1111/j.2153-3490.1974.tb01956.x

Nowack, P. J., Luke Abraham, N., Maycock, A. C., Braesicke, P., Gregory, J. M., Joshi, M. M., & Pyle, J. A. (2015). A large ozone-circulation feedback and its implications for global warming assessments. *Nature Climate Change*, *5*(1), 41–45. https://doi.org/10.1038/nclimate2451

Oberländer, S., Langematz, U., & Meul, S. (2013). Unraveling impact factors for future changes in the Brewer-Dobson circulation. *Journal of Geophysical Research: Atmospheres*, *118*, 10296–10312. https://doi.org/10.1002/jgrd.50775

Oman, L., Waugh, D. W., Pawson, S., Stolarski, R. S., & Newman, P. A. (2009). On the influence of anthropogenic forcings on changes in the stratospheric mean age. *Journal of Geophysical Research: Atmospheres*, *114*, 1–15. https://doi.org/10.1029/2008JD010378

Orbe, C., Rind, D., Jonas, J., Nazarenko, L., Faluvegi, G., Murray, L. T., & Schmidt, G. A. (2020). Giss model e2.2: A climate model optimized for the middle atmosphere–2. validation of large-scale transport and evaluation of climate response. *Journal of Geophysical Research: Atmospheres*, *125*, e2020JD033151. https://doi.org/10.1029/2020JD033151

Orbe, C., Waugh, D. W., Newman, P. A., & Steenrod, S. (2016). The transit-time distribution from the northern hemisphere midlatitude surface. *Journal of the Atmospheric Sciences*, *73*(10), 3785–3802. https://doi.org/10.1175/JAS-D-15-0289.1

Park, M., Randel, W. J., Gettelman, A., Massie, S. T., & Jiang, J. H. (2007). Transport above the Asian summer monsoon anticyclone inferred from Aura Microwave Limb Sounder tracers. *Journal of Geophysical Research*, *112*. https://doi.org/10.1029/2006jd008294

Pascale, S., Carvalho, L. M., Adams, D. K., Castro, C. L., & Cavalcanti, I. F. (2019). Current and future variations of the monsoons of the Americas in a warming climate. *Current climate change reports*, *5*(3), 125–144. https://doi.org/10.1007/s40641-019-00135-w

Phlips, P. J., & Gill, A. E. (1987). An analytic model of the heat-induced tropical circulation in the presence of a mean wind. *Quarterly Journal of the Royal Meteorological Society*, *113*(475), 213–236. https://doi.org/10.1002/qj.49711347513
Popovic, J. M., & Plumb, R. A. (2001). Eddy shedding from the upper-tropospheric Asian monsoon anticyclone. *Journal of the Atmospheric Sciences*, *58*(1), 93–104. https://doi.org/10.1175/1520-0469(2001)058<0093:esftut>2.0.co;2
Qu, X., & Huang, G. (2020). CO_2-induced heat source changes over the Tibetan Plateau in boreal summer-part II: The effects of CO_2 direct radiation and uniform sea surface warming. *Climate Dynamics*, *55*(5–6), 1631–1647. https://doi.org/10.1007/s00382-020-05349-5
Randel, W. J., & Park, M. (2006). Deep convective influence on the Asian summer monsoon anticyclone and associated tracer variability observed with Atmospheric Infrared Sounder (AIRS). *Journal of Geophysical Research*, *111*, 1–13. https://doi.org/10.1029/2005JD006490
Randel, W. J., Zhang, K., & Fu, R. (2015). What controls stratospheric water vapour in the NH summer monsoon regions? *Journal of Geophysical Research: Atmospheres*, 7988–8001. https://doi.org/10.1002/2015JD023622
Ren, R., Zhu, C., & Cai, M. (2019). Linking quasi-biweekly variability of the south Asian high to atmospheric heating over Tibetan plateau in summer. *Climate Dynamics*, *53*. https://doi.org/10.1007/s00382-019-04713-4
Ridley, J., Menary, M., Kuhlbrodt, T., Andrews, M., & Andrews, T. (2019a). *MOHC HadGEM3-GC31-LL model output prepared for CMIP6 CMIP abrupt-4xCO$_2$*. https://doi.org/10.22033/ESGF/CMIP6.5839
Ridley, J., Menary, M., Kuhlbrodt, T., Andrews, M., & Andrews, T. (2019b). *MOHC HadGEM3-GC31-LL model output prepared for CMIP6 CMIP piControl*. https://doi.org/10.22033/ESGF/CMIP6.6294
Rind, D., Lerner, J., Perlwitz, J., McLinden, C., & Prather, M. (2002). Sensitivity of tracer transports and stratospheric ozone to sea surface temperature patterns in the doubled CO_2 climate. *Journal of Geophysical Research*, *107*(24). https://doi.org/10.1029/2002JD002483
Rind, D., Shindell, D., Lonergan, P., & Balachandran, N. K. (1998). Climate change and the middle atmosphere. Part III: The doubled CO_2 climate revisited. *Journal of Climate*, *11*(5), 876–894. https://doi.org/10.1175/1520-0442(1998)011<0876:CCATMA>2.0.CO;2
Schiemann, R., Lüthi, D., & Schär, C. (2009). Seasonality and interannual variability of the westerly jet in the Tibetan plateau region. *Journal of Climate*, *22*(11), 2940–2957. https://doi.org/10.1175/2008JCLI2625.1
Schoeberl, M. R., Pfister, L., Wang, T., Kummer, J., Dessler, A. E., & Yu, W. (2020). Erythemal radiation, column ozone, and the North American monsoon. *Journal of Geophysical Research: Atmospheres*, *125*, e2019JD032283. https://doi.org/10.1029/2019JD032283
Seferian, R. (2018a). *CNRM-CERFACS CNRM-ESM2-1 model output prepared for CMIP6 CMIP for experiment abrupt-4xCO$_2$*. https://doi.org/10.22033/ESGF/CMIP6.3918
Seferian, R. (2018b). *CNRM-CERFACS CNRM-ESM2-1 model output prepared for CMIP6 CMIP piControl*. https://doi.org/10.22033/ESGF/CMIP6.4165
Shaw, T. A., & Voigt, A. (2015). Tug of war on summertime circulation between radiative forcing and sea surface warming. *Nature Geoscience*, *8*(7), 560–566. https://doi.org/10.1038/ngeo2449
Shepherd, T. G. (2008). Dynamics, stratospheric ozone, and climate change. *Atmosphere-Ocean*, *46*(1), 117–138. https://doi.org/10.3137/ao.460106
Sherwood, S. C., Bony, S., Boucher, O., Bretherton, C., Forster, P. M., Gregory, J. M., & Stevens, B. (2015). Adjustments in the forcing-feedback framework for understanding climate change. *Bulletin of the American Meteorological Society*, *96*(2), 217–228. https://doi.org/10.1175/BAMS-D-13-00167.1
Sigmond, M., Siegmund, P. C., Manzini, E., & Kelder, H. (2004). A simulation of the separate climate effects of middle-atmospheric and tropospheric CO_2 doubling. *Journal of Climate*, *17*(12), 2352–2367. https://doi.org/10.1175/1520-0442(2004)017<2352:ASOTSC>2.0.CO;2
Siu, L. W., & Bowman, K. P. (2019). Forcing of the upper-tropospheric monsoon anticyclones. *Journal of the Atmospheric Sciences*, *76*(7), 1937–1954. https://doi.org/10.1175/JAS-D-18-0340.1
Staudt, A. C., Jacob, D. J., Logan, J. A., Bachiochi, D., Krishnamurti, T. N., & Sachse, G. W. (2001). Continental sources, transoceanic transport, and interhemispheric exchange of carbon monoxide over the Pacific. *Journal of Geophysical Research*, *106*(D23), 32571–32589. https://doi.org/10.1029/2001JD900078
Stolarski, R. S., Waugh, D. W., Wang, L., Oman, L. D., Douglass, A. R., & Newman, P. A. (2014). Seasonal variation of ozone in the tropical lower stratosphere: Southern tropics are different from northern tropics. *Journal of Geophysical Research: Atmospheres*, *119*, 6196–6206. https://doi.org/10.1002/2013JD021294
Tang, Y., Rumbold, S., Ellis, R., Kelley, D., Mulcahy, J., Sellar, A., & Jones, C. (2019a). *MOHC UKESM1.0-LL model output prepared for CMIP6 CMIP abrupt-4xCO$_2$*. https://doi.org/10.22033/ESGF/CMIP6.5843
Tang, Y., Rumbold, S., Ellis, R., Kelley, D., Mulcahy, J., Sellar, A., & Jones, C. (2019b). *MOHC UKESM1.0-LL model output prepared for CMIP6 CMIP piControl*. https://doi.org/10.22033/ESGF/CMIP6.6298
Tweedy, O. V., Waugh, D. W., Randel, W. J., Abalos, M., Oman, L. D., & Kinnison, D. E. (2018). The impact of boreal summer ENSO events on tropical lower stratospheric ozone. *Journal of Geophysical Research: Atmospheres*, *123*, 9843–9857. https://doi.org/10.1029/2018JD029020
Tweedy, O. V., Waugh, D. W., Stolarski, R. S., Oman, L. D., Randel, W. J., & Abalos, M. (2017). *Hemispheric differences in the annual cycle of tropical lower stratosphere transport and tracers.*, 1–17. https://doi.org/10.1002/2017JD026482
Vera, A., Higgins, W., Amador, J., Ambrizzi, T., Garreaud, R., Gochis, D., et al. (2006). Toward a unified view of the American monsoon systems. *Journal of Climate*, *19*(20), 4977–5000. https://doi.org/10.1175/JCLI3896.1
Voldoire, A. (2018a). *CMIP6 simulations of the CNRM-CERFACS based on CNRM-CM6-1 model for CMIP experiment abrup-4xCO2*. https://doi.org/10.22033/ESGF/CMIP6.4163
Voldoire, A. (2018b). *CMIP6 simulations of the CNRM-CERFACS based on CNRM-CM6-1 model for CMIP experiment piControl*. https://doi.org/10.22033/ESGF/CMIP6.4163
Wang, B., & Ding, Q. (2008). Global monsoon: Dominant mode of annual variation in the tropics. *Dynamics of Atmospheres and Oceans*, *44*(3–4), 165–183. https://doi.org/10.1016/j.dynatmoce.2007.05.002
Wang, B., Liu, J., Kim, H. J., Webster, P. J., Yim, S. Y., & Xiang, B. (2013). Northern Hemisphere summer monsoon intensified by mega-El Niño/southern oscillation and Atlantic multidecadal oscillation. *Proceedings of the National Academy of Sciences of the United States of America*, *110*(14), 5347–5352. https://doi.org/10.1073/pnas.1219405110
Wang, K.-Y., & Shallcross, D. E. (2000). A modelling study of tropospheric distributions of the trace gases CFCl. *Annales Geophysicae*, *18*(8), 0972. https://doi.org/10.1007/s005850050013
Webster, P. J. (1972). Response of the tropical atmosphere to local, steady forcing. *Monthly Weather Review*, *100*(7), 518–541. https://doi.org/10.1175/1520-0493(1972)100<0518:ROTTAT>2.3.CO;2
Xia, Y., Huang, Y., & Hu, Y. (2018). On the climate impacts of upper tropospheric and lower stratospheric ozone. *Journal of Geophysical Research: Atmospheres*, *123*, 730–739. https://doi.org/10.1002/2017JD027398

Yan, X., Konopka, P., Ploeger, F., Tao, M., Müller, R., Bian, J., & Riese, M. (2018). El Niño Southern Oscillation influence on the Asian summer monsoon anticyclone. *Atmospheric Chemistry and Physics Discussions*, 1–25. https://doi.org/10.5194/acp-2017-1135

Yongfu, Q., Qiong, Z., Yonghong, Y., & Xuehong, Z. (2002). Seasonal variation and heat preference of the south Asia high. *Advances in Atmospheric Sciences*, *19*(5), 821–836. https://doi.org/10.1007/s00376-002-0047-3

Yukimoto, S., Koshiro, T., Kawai, H., Oshima, N., Yoshida, K., Urakawa, S., & Adachi, Y. (2019a). *MRI MRI-ESM2.0 model output prepared for CMIP6 CMIP abrupt-4xCO$_2$*. https://doi.org/10.22033/ESGF/CMIP6.6755

Yukimoto, S., Koshiro, T., Kawai, H., Oshima, N., Yoshida, K., Urakawa, S., & Adachi, Y. (2019b). *MRI MRI-ESM2.0 model output prepared for CMIP6 CMIP piControl*. https://doi.org/10.22033/ESGF/CMIP6.6900